Deliverable Report

Deliverable No: D2.1

Deliverable Title: Architecture for femtosecond laser-written platform

Grant Agreement number: 899544

Project acronym: PHOQUSING

Project title: PHOtonic Quantum SamplING machine

Project website address: www.phoqusing.eu

Name, title and organisation of the scientific representative of deliverable's lead beneficiary (task leader):
Prof. Fabio Sciarrino, Università di Roma "La Sapienza"
Email: fabio.sciarrino@uniroma1.it

Deliverable table

Deliverable no.	D2.1
Deliverable name	Architecture for femtosecond laser-written platform
WP no.	2
Lead beneficiary	UNIROMA1
Type	Report
Dissemination level	Public
Delivery date from Annex I	M18
Actual delivery date	28 February 2022

What was planned *(from Annex I:)*

D2.1: Architecture for femtosecond laser-written platform [18]
Report on the definition of the most appropriate architecture for integrated circuits based on the laser-writing technology, for manipulation of multiphoton states. Peculiar properties of the fabrication technique, such as polarization control and three-dimensional capabilities, will be included in the analysis.

What was done

One of the advantages of photonic platforms in quantum information processing is the possibility to decompose any unitary transformation of single- and multi-photon states in a sequence of elementary linear optical units. In literature, two universal schemes have been proposed to realize any transformation by means of beam splitters and phase shifters [Reck1994, Clements2016]. These methods have found straightforward experimental implementations in integrated photonic devices, which offer in addition the ability to reconfigure the circuit by exploiting tunable phase shifters. Furthermore, these architectures present the possibility of being at the same time programmed, to reach a specific unitary operation, as well as drawing Haar random matrices for sampling-based algorithms. In parallel, this discrete decomposition requires a certain number of layers to implement arbitrary transformations, and thus sensitivity to errors and photon losses must be taken into account. Crucial aspects regard indeed the scaling of the optical elements and of the circuit depth required to realize *m*-port interferometers.
The femtosecond laser-writing technology presents the unique capability of enabling 3-dimensional architectures for waveguide fabrication. This enables the possibility of fabricating arrays of several waveguides placed parallel one to each other, and are continuously coupled by evanescent-field interaction. This represents a promising approach to implement large scale circuits with a more favorable scaling with respect to losses and fabrication imperfections. However, in the literature there is still not a systematic and complete study on the universality of such approach for multi-mode interferometers fabrication.
In Deliverable 2.1 we have analyzed these two architectures as the most appropriate to implement large reconfigurable circuits with the femtosecond laser-writing technology.

Continuously-coupled architectures

We investigated as possible solutions the continuous-coupling model of radiation among waveguides arranged in 1D or 2D lattices (see Figure 1).

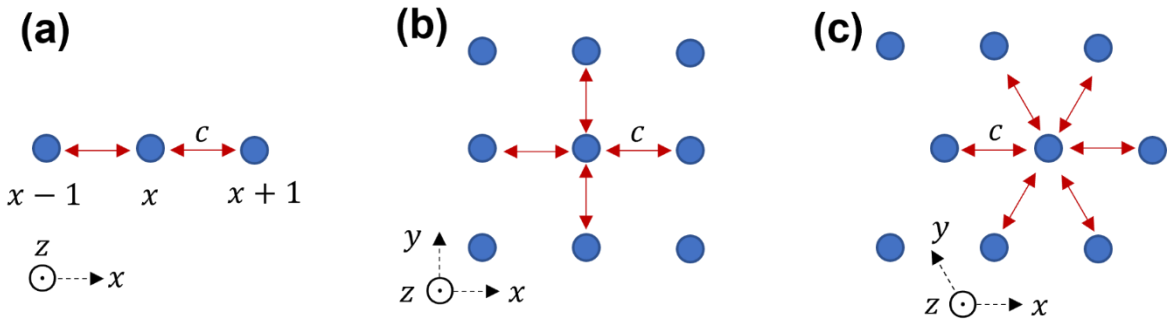

Figure 1. Cross section of waveguide lattices. The time coordinate of the evolution corresponds to the propagation axis z perpendicular to the figure plane. (a) One dimensional lattice, (b) rectangular lattice and (c) triangular lattice. In the latter geometry each site has the largest number of first neighbors. It is the more compact structure in terms of circuit length and thus of photon insertion losses.

In this approach the geometry of the lattice determines the Hamiltonian H of the system. The latter can be expressed in terms of the annihilation and creation operators of the electromagnetic field as

$$H = \sum_i k_i \, a_i^\dagger a_i \; + \sum_{i \neq j} c_{ij} a_i^\dagger a_j \qquad (1)$$

where the k_i are the site energies, and the coefficients c_{ij} are the coupling coefficients among neighbor sites. Then, the equation that regulates the propagation of the field in the circuit considering

only first neighboring interactions, i.e interactions among sites that are distant from each other by one lattice pitch d, will be

$$-i\frac{da_x}{dz} = k_x a_x + \sum_{|i-x|=d} c_{xi} a_i \qquad (2)$$

where z is the axis of light propagation that here has the role of the time coordinate. In all the calculations we consider $\hbar = 1$.

Minimum circuit length

Our first study aimed at finding the optimal geometry of continuously-coupled circuits that minimizes the circuit length L_m required to have a nonzero probability to reach any site of the lattice starting the propagation from any optical mode. To this aim we solved Eq. (2) for the one-dimensional lattice (Figure 1a) and for two 2D geometries, the square (Figure 1b) and triangular one (Figure 1c). In this calculation we consider for simplicity constant $c_{ij} = c$, since we are mainly interested at finding the scaling of L_m with respect to the number of optical modes m. From our study, the triangular arrangement resulted to be the most compact structure in terms of the light spreading. In particular, we find that $L_m \sim \sqrt{m}$. Same considerations on the circuit minimum length can be applied to the discrete architectures. The comparison between the two types of integrated circuits is useful to understand the actual gain of the adoption of continuously-coupled waveguides. The estimation of L_m was performed for discrete circuits that follow the most recent decomposition scheme by Clements et al. [Clements2016]. Here, we considered the length of each beam-splitter and phase-shifter, realized in their integrated counterparts as directional couplers and as bending of the waveguides respectively. It follows that in this case $L_m \sim m$.

Further advantages can be found in the design of the fan-in and fan-out regions that link the circuit to the external fiber arrays. It is important to study how the length scales also for these parts of the circuit. In fact, we should at least check that advantages in compactness gained in the interferometer section are not vanished by long fan-in and fan-out sections. We found that as the number of modes increases, the length of these sections tends to be less relevant than the length of a Clements interferometer since it scales as $\sim \sqrt{m}$. Thus, it shares a similar scaling law as a three-dimensional continuously-coupled interferometer. An improved compactness may be gained if the m fibers to be coupled are arranged on a two-dimensional grid, as in the devices reported in Figure 2. Note that such

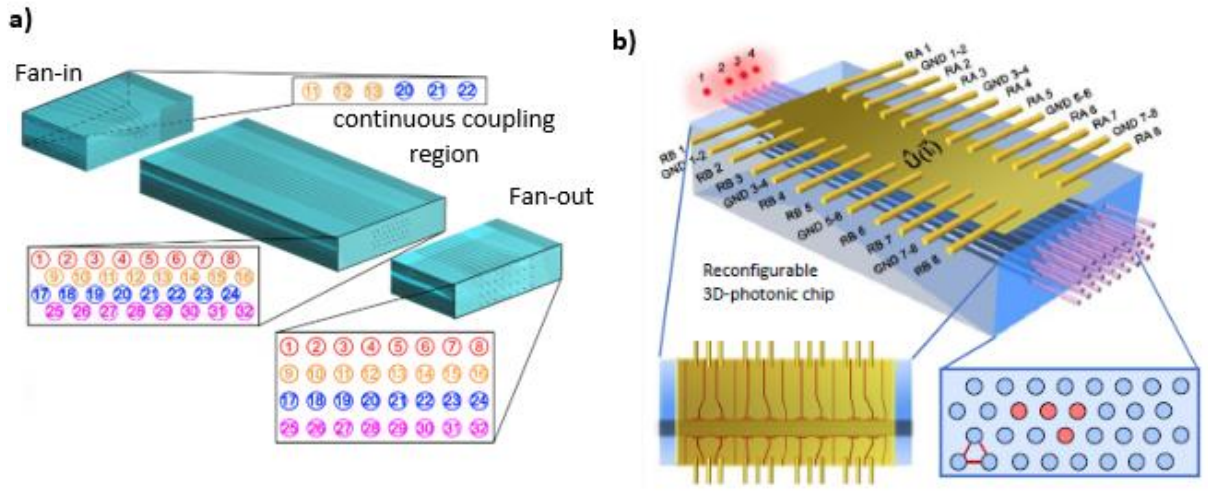

Figure 2. Examples of continuously-coupled optical circuits. a) Static 32-mode circuit based on the coupling among waveguides arranged in a 3D layout. The lattice displays a 2D triangular cross section in the transverse plane. In the scheme are highlighted the interaction region and the fan-in and fan-out to connect the chip with external fibers. b) Reconfigurable version of the circuit with 16 heaters that allows to change the unitary transformation implemented in the optical circuit. Figure b from Ref. [Hoch2021].

a configuration can be realized only in the 2D continuously-coupled architectures. In this scenario the maximum size of the fiber array cross-section, in either dimension, scales as $\sim \sqrt{m}$. It follows that the length of the fan-in or fan-out section here scales as $\sqrt[4]{m}$. This further contributes to limiting the device footprint and, hence, its optical insertion losses.
As a practical example, we report in Figure 2a a 32-mode continuously-coupled optical circuit arranged in a 2D triangular cross-section lattice. The circuit was realized through the femtosecond laser writing (FLW) technique of waveguides. For what concerns analogous apparatuses realized according to the Clements decompositions, the length of the optical units strongly depend on the fabrication technology of the waveguides. We considered the FLW for a fair comparison between the two schemes. The device in Figure 2a requires a 7.5-cm long optical chip, while the discretely coupled interferometer with the same number of modes produced with the same technology would have required a device length of about 30 cm [Hoch2021].

Unitary transformations
The unitary transformation U that represents the operation of the optical circuit derives from the integration of the Hamiltonian in Eq. (1) over the interaction length, i.e. the circuit portion in which the waveguides exchange the radiation. Despite the aforementioned advantages in terms of circuit compactness, a general algorithm has still to be devised that provides a recipe on how to implement an arbitrary unitary transformation of the optical modes with this kind of device. All previous considerations to individuate the optimal design of the lattice regard homogeneous arrays, in which coupling coefficients are uniform across the array and along the waveguide direction. In addition, the evaluation of circuit lengths has been carried out only by considering the spreading of the light to all output waveguides, with no constraints on the unitary transformation provided by the circuit. As a matter of fact, homogeneous arrays produce highly symmetric transformations, which may not preserve for instance the complexity of the Boson Sampling problem that requires random extracted unitary circuits.
We have then investigated the conditions necessary to implement a random unitary transformation in a continuously coupled architecture. They can be summarized as follows:

- *Modulation of propagation constants.* Previous theoretical works [Banchi2017] have shown that a random time-modulation of the site energies, in a quantum walk on a one-dimensional chain of sites, is able to provide Haar-random transformations of the input states in the long-time scale. In a photonic setting, such a quantum walk can be implemented by a photon propagating in planar waveguide arrays, where the propagation constant k_i of the waveguides is modulated randomly along the z direction, and in a different way in each waveguide, i.e $k_i = k + \Delta k_i(z)$. A random transformation would then be achieved with a sufficiently long device, as recently experimentally demonstrated in a square and linear lattice geometries [Tang2021].

- *Modulation of coupling coefficients.* As further investigation developed in this deliverable, we made some consideration regarding the modulation of the parameters c_{ij} in Eq. (1). Random matrices can be obtained by applying small displacements to the waveguide positions from the lattice. In the simulation, the propagation constants were kept homogeneous $k_i = k$ for simplicity, while $c_{ij} = c + \Delta c_{ij}(z)$. The deviations Δc_{ij} reflect the changes in the waveguide distances introduced for example by the random displacements along the propagation axis (see Ref. [Hoch2021]).

Modulating the physical parameters

We have investigated the modulations of the parameters that control the evolution through a continuously-coupled optical circuit in order to individuate the condition of the Haar randomness. We focused on the two 2D lattices, the square and the triangular ones, which can be implemented only via a 3D geometry of waveguides fabrications. The aim of the following simulations was to individuate the optimal design to realize Haar-random evolutions in the most compact way. We use as a figure of merit of the achieved randomness the quantity proposed in [Tang2021]. It is defined as the L_2-distance between the single-photon probability distribution $|U_{ji}|^2$ in the outputs j given the input i, and the uniform distribution $\frac{1}{m}$, where m is the number of the lattice sites. In Figure 3 we consider $m = 32$ arranged in 4 columns and 8 rows according with the square and triangular lattices geometries. Such a figure of merit for 32x32 Haar-random matrices, averaged on 200 extractions, is around 0.1665. In the first two colormaps the value of the distance has been reported for different values of the detuning Δk. In these circuits the couplings among first neighbor waveguides have been kept constant while the time evolution has been discretized in time steps of $\Delta z = 4mm$. The k coefficients have been uniformly and independently extracted in the range Δk at each step. It is worth noting that the triangular geometry displays a better convergence towards the Haar-random matrices with respect the propagation length L. This is confirmed also in the case of the same kind of modulation of the parameters c with static propagation constants (the two plots below). Although this analysis can highlight some of the advantages of the triangular geometry, such figure of merit for the randomness is not conclusive. As further investigation, we report in Figure 4 an insight regarding the histograms of phases, moduli and similarity among distributions $|U_{ji}|^2$ of the unitaries after a propagation length of $L = 36mm$ and $\Delta k = 0.25mm^{-1}$ a) and $\Delta c = 0.125mm^{-1}$ b). These conditions for extracting the transformations corresponds to an intermediate scenario in which the convergence towards the Haar-randomness is not completely reached. In Figure 4a it is evident the better convergence of the triangular lattice when compared with the analogous square circuit. From this further analysis emerges that the modulation of the couplings in the square lattice generates matrices very far from the Haar-random sampling (see Figure 4b). The reason behind this evident deviation from the triangular lattice could be the smaller number of first neighbors for each site (4 vs 6) and, consequently the number of couplings parameters (52 vs 73). In addition, the arrangement of the lattice in the 8x4 rectangular grid could break the symmetry of the square lattice which is not broken in the triangular case instead.

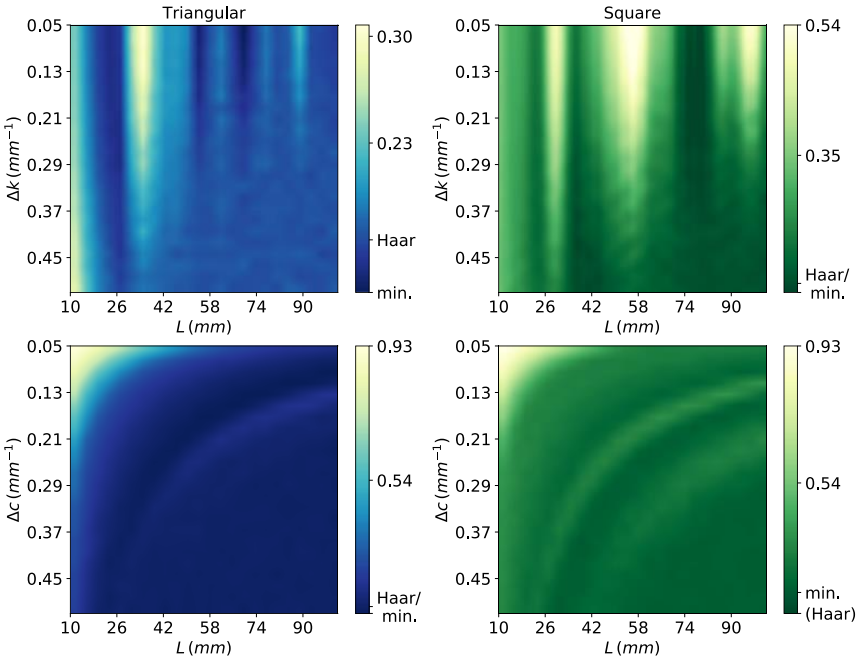

Figure 3. Distance from the uniform distribution of the one photon evolutions in the triangular (blu scale) and square (green scale) lattices. In the first row we report the distances for the randomness introduced in the propagation constants, for different values of the amplitudes Δk and circuit length L. The same analysis for the randomness in the Δc. In all colorbars the minimum values of the distances are highlighted and compared with the Haar value.

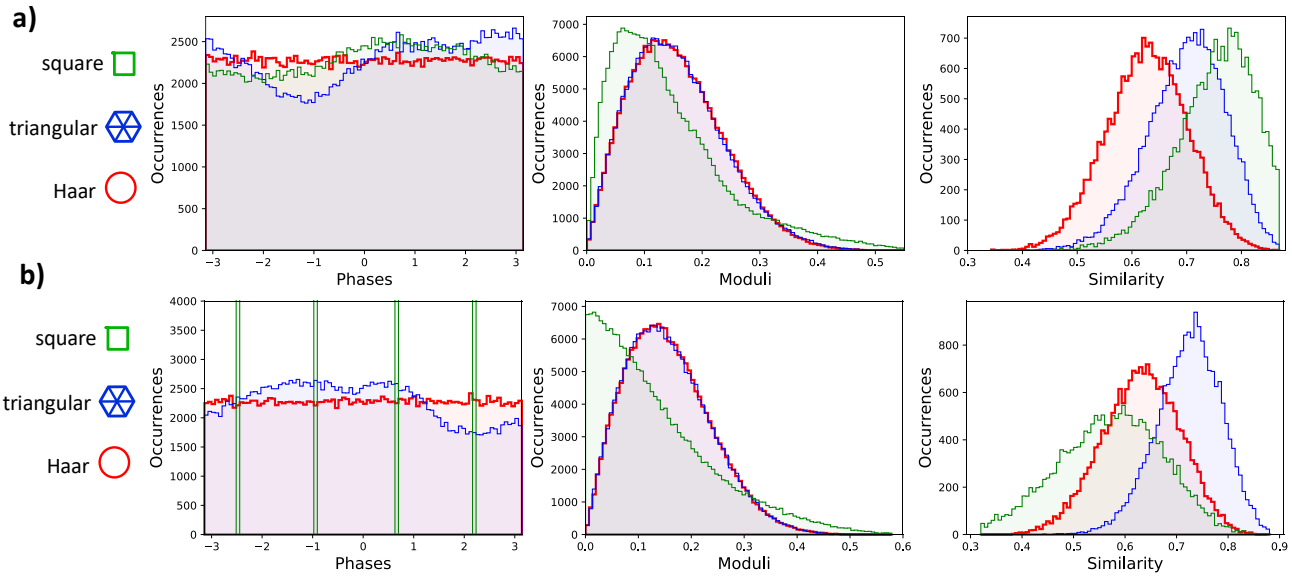

Figure 4 a) Distributions on the phases, moduli and squared moduli columns of the unitary matrices generated by square (green) and triangular (blue) lattice compared with the Haar-random matrices (red). In this simulation we sampled 200 configurations of propagation constants in the range $\Delta k = 0.25mm^{-1}$, constant couplings $c = 0.2mm^{-1}$, in time steps of $\Delta z = 4mm$, for a total propagation of $L = 36mm$. b) Same analysis for the coupling coefficients. Here they were sampled in the range $\Delta c = 0.125mm^{-1}$, while $k = 0.2mm^{-1}$.

In summary, the triangular geometry results to be the most convenient for what concerns the light spreading (see previous section), and for implementing random evolution in the most compact and robust way. The modulations of the Hamiltonian investigated in this section can be performed in various way during the fabrication stage of the optical circuit. For example, the random modulations $\Delta k(z)$ have been realized in square and linear lattices with the femtosecond-laser writing technique [Gattas2008] by changing the writing speed of the waveguides (see Ref. [Tang2021]). In PHOQUSING we modulated the couplings $\Delta c(z)$ by slight displacements of the waveguides positions from a triangular lattice. This methodology can reproduce only static circuit or, equivalently, a single unitary transformation. In the following section we are going to illustrate a way to introduce dynamical modulation of the circuit parameters and thus obtain a reconfigurable device able to realize several Haar-random matrices.

Towards reconfigurable continuously-coupled circuits.

Starting from the above discussion we realized the reconfigurable circuit reported in Figure 2b, with the aim to implement several random generated unitary transformations [Hoch2021]. Before going into the details of the physical device, we show some numerical results regarding the actual possibility to realize reconfigurable circuits by means of heaters and the thermo-optic effect.

In fact, the refractive index of the waveguide changes with the temperature. In integrated optical circuits phase shifts are realized through micro-resistive materials placed nearby the waveguide location. The dissipated electrical powers in the resistors induce a change in the refractive index of the waveguide and thus in the corresponding propagation constant. We have seen that to reach a good randomness it is necessary to tune individually each parameter k. This is not trivial to realize since it would require placing heaters inside the waveguide lattice. The solution that we have found in PHOQUSING is to exploit the static randomness provided by the modulation of the $c_{ij}(z)$ during the fabrication process of the triangular lattice, combined with a dynamic modulation of the $k_i(z)$ by a sequence of heaters placed on the top surface of the circuit. These heaters cannot in principle influence individually and independently each waveguide. Notwithstanding, a reasonable number of heaters along the propagation axis, together with an appropriate arrangement, allow us to sample

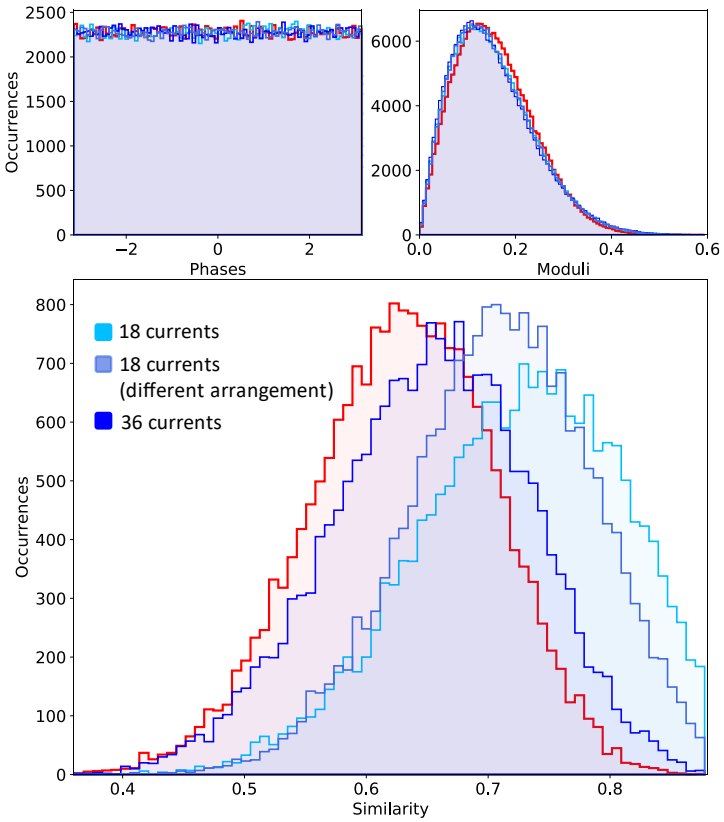

Figure 5 Reconfigurable continuously coupled circuits in the triangular lattice arrangements. Appropriate settings of heaters on the top surface enable to reproduce Haar-random matrices in a reconfigurable way. The matrix are obtained by uniform sampling of the dissipated electrical power generated by the currents applied to the heaters.

matrices very close to the Haar-random measure. In Figure 5 we report our results for what concerns the phases, moduli and similarity distribution for such kinds of circuit. In this simulation we consider again 8x4 triangular lattice with a propagation length of $L = 36mm$, divided in 9 time steps in which the couplings have been modulated according to one extraction of $c_{ij}(z)$ within an interval of amplitude $\Delta c = 0.125mm^{-1}$. In the light blue color the results when 9 heaters are placed per side on the top surface, for a total of 18 control parameters (the applied electrical currents). This means that each of them influences directly the 4 waveguides placed under the heaters for a length of $\Delta z = 4mm$. The other propagation constants are modified by considering a linear gradient of the temperature inside the lattice. The histograms correspond to 200 uniformly distributed Δk up to $1mm^{-1}$ that it is equivalent to a random uniform extraction of the dissipated powers in the heaters. It is worth noting that, while the phases and the moduli distributions are in perfect agreement with the Haar matrices, the overlap between the histograms of the similarity is not optimal. This can be improved by changing the arrangement of the heaters on the top surface (middle-blue data) and by increasing their numbers (blue data). In the middle-blue case we consider odd time steps with two heaters per side like in the light blue configuration. In the even time steps, one heater controls the central four waveguide while the remaining four (two per side) are controlled by the other dissipated power. For the last case, that best reproduces the Haar-sampling, four heaters at each time steps are placed on the top and control two waveguides each. We remind that for this kind of architectures it does not exist an algorithm that tells how to link the dissipated powers to the matrix elements. The findings presented in this deliverable are one of the first numerical investigation in this direction. Note that in the discrete-decomposition schemes there exist already algorithms to set the optical circuit to sample from the Haar distribution. However, the phase shift values and beamsplitter reflectivities do not display trivial distributions which in turn require complex settings of the external control circuit. More precisely, by increasing the dimension of the matrix, the parameter distributions tend to be more and more peaked [Burgwal2017, Russell2017]. For example, the uniform sampling of the dissipated electrical powers employed in our investigation is far from the correct sampling to generate random Haar matrices in discrete optical circuits as shown in the numerical simulation of Figure 6.

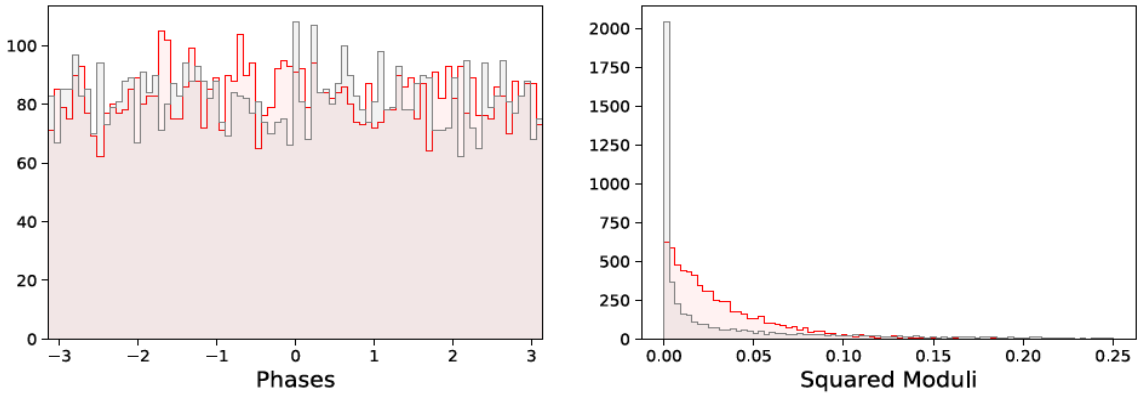

Figure 6. In grey we report the phases and squared moduli distribution of matrix corresponding to Clements circuits in which the internal parameters have been extracted randomly according to a uniform distribution. The squared moduli distribution is not in accordance with the Haar-random matrices trend (red histogram).

Implemented 32-mode device.

We move now to the description of the physical integrated circuit showed in Figure 2b realized in PHOQUSING. The chip comprises 16 resistive micro-heaters patterned on the chip surface. The resistors are equally distributed on the two sides of the interaction region. An external power supply controls the currents applied to the resistors. In addition, we use an array length that is more than twice the estimated minimum length L_m with our experimental parameters, in order to promote further mixing of the light across the waveguide array. The achieved randomness has been investigated experimentally, as described in Figure 6. We have tested the reconfigurability of the system by comparing the sub-matrix reconstructed by injecting single and pairs of photons in three inputs of the device with likewise random sub-matrix extracted from the Haar-distribution. Figure 7 reports the results of the analysis that proves a high level of reconfigurability and a good overlap with the random matrices. In this regard, the first investigation was focused on the distributions of phases

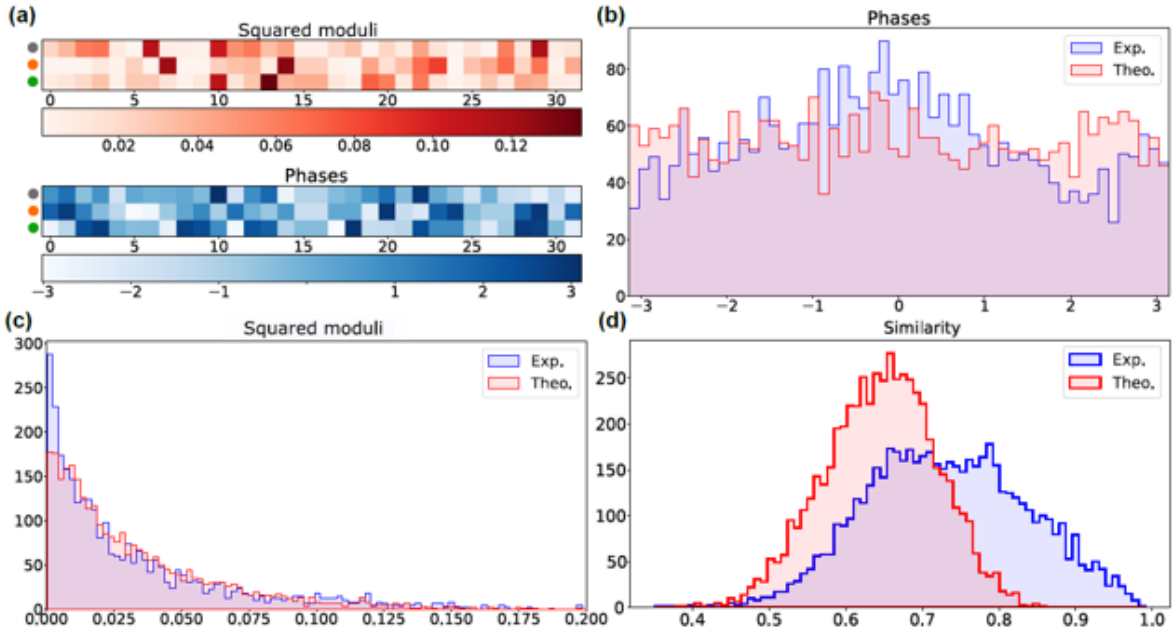

Figure 7. Comparison with Haar-random distribution. a) An example of a 3x32 submatrix reconstructed for a set of electrical currents applied to the heaters. b-c) Comparison of the phases and moduli of the 15 sub-matrix implemented and reconstructed in the experiment with likewise submatrix extracted from the Haar-distribution. d) Histogram of similarities between the squared moduli of columns belonging to experimental implemented transformations (blue) and of similarities between the squared moduli of Haar-random matrix (red). Figure from Ref. [Hoch2021].

and moduli of matrix elements (Figure 7b,c). The second step was to quantify somehow the number of unitary transformations covered by extracting uniformly the electrical power dissipated in the heaters. The histogram in Figure 7d shows in blue the distribution of the similarities between the squared moduli of matrix columns resulting from different sets of dissipated powers and compared with the same quantity estimated for Haar random matrices. The values of the similarities and the overlap (62,4%) with the theoretical histogram of random unitary transformations are very encouraging for the task we are looking for. The latter result represents one of the first experimental investigations on the level of randomness that can be reached in this reconfigurable continuously-coupled waveguide architecture by changing not individually the propagation constants via the thermo-optic effect.

We remind that an exhaustive and conclusive answer regarding the possibility to extract matrices from a distribution closer to the Haar measure with a reconfigurable continuously-coupled waveguide architecture with a given geometry needs further studies both from a theoretical and experimental point of view. For example, future studies within PHOQUSING will focus on methods that allow one to control and program the transformations that the device can implement. This means finding a model that links the parameters of the unitary transformations to the dissipated electrical powers in the heaters, which is a problem still not addressed in the literature for reconfigurable continuously-coupled waveguide circuits. We believe that the use of a black-box approach, via neural networks and optimization algorithms is effective and promising (see also Deliverable 6.1). Further improvements in the reconfigurability could be brought from modifications of the present device architecture, e.g. by increasing the number of heaters and by changing their arrangement with respect to the waveguide positions as we have demonstrated in the numerical simulations.

Discretely-coupled architecture

Architectures based on discretely-coupled waveguides in two-dimensional circuits are well documented in literature [Reck1994, Clements2016]. A design based on a triangular mesh of reconfigurable Mach-Zehnder Interferometers (MZIs) was reported by Reck et al. in 1994, which was followed by a rectangular mesh by Clements et al. in 2016. Both designs are capable of implementing universal transformations, yet Clements' implementation improves on the previous work by halving the total circuit length while reducing differential losses between modes thanks to a more symmetrical geometry (see Figure 8).

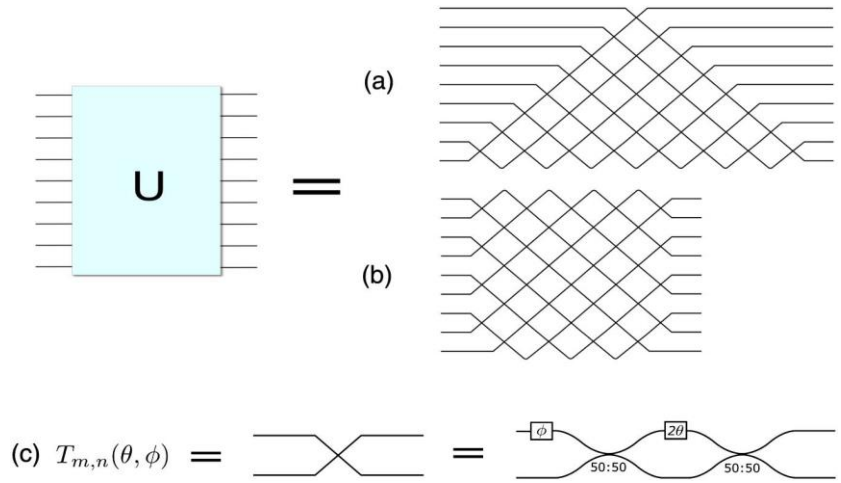

Figure 8. Universal multiport interferometer designs. a) Triangular mesh. b) Rectangular mesh. c) Basic unit cell for both layouts, consisting of two phase shifters and two balanced directional couplers. Figure from Ref. [Clements2016].

The 6-mode universal processor we fabricated features 15 MZIs arranged in the Clements configuration, with a total of 30 thermal phase shifters for its reconfigurability. The thermal phase shifters were fabricated starting from a thin gold film which is deposited on the sample and then

ablated by a femtosecond laser [Ceccarelli2019]. To ensure low power dissipation and low thermal crosstalk among all of these phase shifters the circuit features a total of 60 deep isolation trenches fabricated by water-assisted laser ablation [Ceccarelli2020]. The layout of the universal processor is shown in Figure 9.

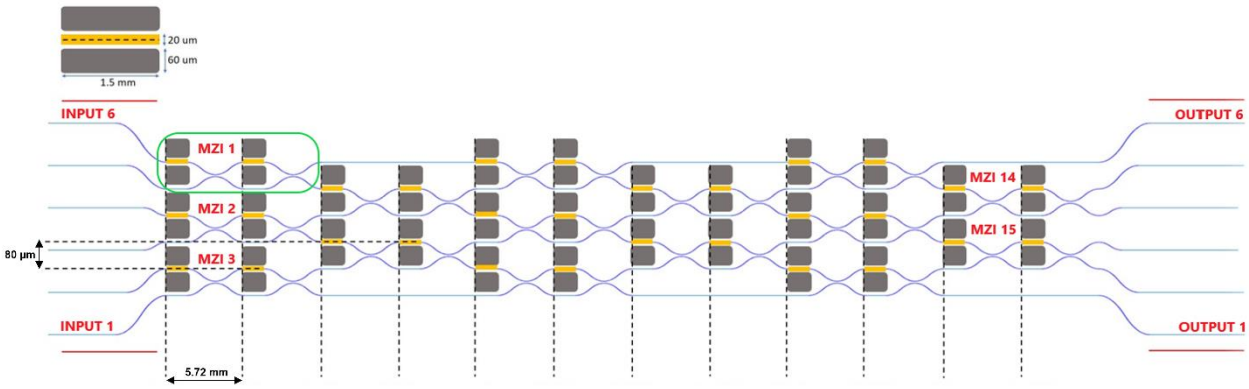

Figure 9. Layout of the 6-mode universal processor. Gray rectangles represent 300 µm deep isolation trenches, yellow rectangles represent the thirty 10 µm wide phase shifters. The basic unit cell is highlighted in the top left by a green line. Fan-in and fan-out are added for compatibility with standard 127 µm fiber arrays.

Optical characterization

The processor features a total 2.7 dB insertion loss at a wavelength of 785 nm. A preliminary characterization of the reconfigurability performance has been carried out by evaluating the power dissipation and thermal crosstalk of the two MZIs closest to the output of the circuit (MZI 14 and MZI 15 as in Figure 7) in both atmospheric pressure and in vacuum. Power dissipation has been characterized in terms of the electrical power necessary for a 2π phase shift ($P_{2\pi}$), while thermal crosstalk is defined as the phase induced on an adjacent MZI as a percentage of the phase induced on the target MZI. These measurements are shown in Table 1: power dissipation for full reconfigurability in atmospheric pressure is about 30 mW, while thermal crosstalk is of the order of 15%. At a pressure of 2.5×10^{-3} mbar these values drop respectively to 11 mW and 2%.

Pressure	Measure	MZI 14	MZI 15
ATM	$P_{2\pi}$ (mW)	36	28
ATM	Crosstalk (%)	22.3	13.4
2.5×10^{-3} mbar	$P_{2\pi}$ (mW)	11.5	11
2.5×10^{-3} mbar	Crosstalk (%)	2.5	1.9

Table 1. Characterization of power dissipation and thermal crosstalk in standard conditions and in vacuum for the two rightmost MZIs of the 6-mode processor.

The optical power at the bar output of an ideal MZI can be modeled as:

$$\mathcal{P}_{out} = \frac{1 - \cos(\phi + \phi_0)}{2}, \qquad (3)$$

where ϕ is the phase shift induced by the internal phase shifter and ϕ_0 is the initial phase of the interferometer, which is randomly determined during fabrication and has to be characterized for each individual MZI in order to properly control the universal processor. There is a linear relation between induced phase and electrical power dissipated on the thermal phase shifter P: $\phi = \alpha P$. In practice however, we control these devices by imposing a current I instead of an electrical power; for this reason we need to make some further considerations.

While the electrical power is related to the current by the resistance as RI^2, the resistance itself depends on the current, hence we must include a higher order term in the electrical power: $P = R_0 I^2 + \beta I^4$, where R_0 is the resistance of the phase shifter at room temperature and β is a non-linear factor which accounts for this dependence of resistance on the current. Furthermore, due to thermal crosstalk, the phase shift ϕ_i imposed by the i-th phase shifter effectively depends on the electrical power dissipated on all the other phase shifters P_j as:

$$\phi_i - \phi_{0,i} = \sum_j \alpha_{ij} P_j. \tag{4}$$

In general, the matrix α_{ij} has dimensions equal to the number of phase shifters on the circuit. However, we assume that the horizontal thermal crosstalk between phase shifters on different columns can be neglected due to the large distance between them (in the order of millimeters due to the curvature radius of FLW waveguides, see Figure 9). This assumption significantly simplifies the matrix α_{ij} and reduces the number of measurements required to characterize and compensate the effect of thermal crosstalk.

Switching unitary transformations

The calibration procedure adapted from literature [Clements2016] has been performed along with initial measurements involving the implementation of unitary transformations. We implemented three types of switching unitaries: the 6 integer powers of the 6-dimensional Pauli-X gate, 4 switching unitaries (from input 2 to outputs 3-6) and 10 random permutations (see Figure 10). The fidelity of each of these unitary transformations has been calculated as:

$$\mathcal{F}(M_{exp}, M) = \frac{1}{6} tr(M_{exp}^{\dagger}, M), \tag{5}$$

where M is the ideal unitray matrix implemented and M_{exp} is the measured unitary.
The average fidelity for all of the unitaries measured is equal to $\mathcal{F}_{avg} \pm \sigma = 0.99676 \pm 0.00048$.

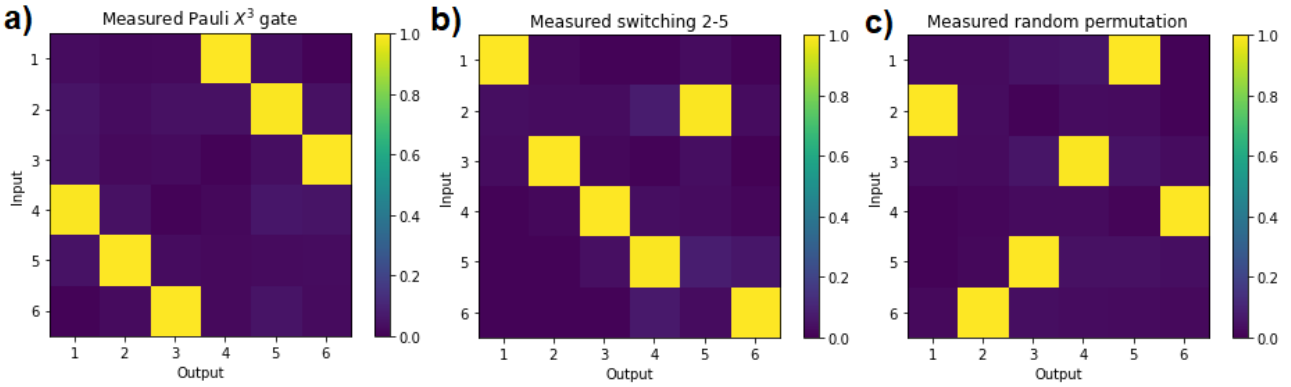

Figure 10. Measured switching unitary transformations on 6-mode processor. a) Pauli X^3gate. b) Switching unitary from input 2 to output 5. c) Random permutation.

Bibliography

[Banchi2017] L. Banchi et al., Phys. Rev. X **7**, 041015 (2017)
[Burgwal2017] R. Burgwal, et al., Opt. Express **25**, 28236 (2017).
[Ceccarelli2019] F. Ceccarelli et al., J. Light. Technol. **37**, 4275–4281 (2019)
[Ceccarelli2020] F. Ceccarelli et al., Laser Photonics Rev. **14**, 2000024 (2020)
[Clements2016] W. R. Clements et al., Optica **3,** 1460 (2016)
[Gattas2008] R. R. Gattass and E. Mazur, Nature Photonics **2**, 219 (2008).
[Hoch2021] F. Hoch et al., arXiv:2106.08260 [quant-ph] (2021)
[Reck1994] M. Reck et al., Phys. Rev. Lett. **73**, 58 (1994)
[Russell2017] N. J. Russell et al. New J. Phys. **19**, 033007 (2017).
[Tang2021] H. Tang et al., arXiv:2112.06549 [quant-ph] (2021)